

# Precise Capillary-Assisted Nanoparticle Assembly in Reusable Templates

Henry S. C. Yu, Ana Conde-Rubio, Hsiang-Chu Wang, Olivier J. F. Martin, Giovanni Boero, and Jürgen Brugger\*

Capillary-assisted particle assembly (CAPA) in predefined topographical templates is a scalable method for the precise positioning of nanoscale objects on various surfaces. High-resolution CAPA templates are typically fabricated by expensive electron-beam lithography and are used for a single assembly process. To increase the scalability and reduce the costs of the CAPA technique, the fabrication and characterization of reusable templates with nanoscale funnel-shaped traps for repetitive precise nanoparticle placement are demonstrated. The yield of the first assembly of 100 nm gold nanoparticles (AuNPs) is as high as 94% with a median position offset of about 10 nm. The subsequent transfer process of the AuNPs from the silicon assembly template onto polymer surfaces, such as the elastic polydimethylsiloxane or the inelastic OrmoComp, shows a transfer yield larger than 99%. After the first transfer process, the assembly template is reused, resulting in a position offset and an assembly and transfer yield of this second assembly/transfer step that are comparable to the first ones. The obtained results demonstrate that the nanotemplates made by electron-beam lithography can be reused for repeatable CAPA processes and thereby eliminate the need for recurring lithography steps for each assembly and thus make the CAPA technique more cost-efficient.


## 1. Introduction

Nanoparticles have become one of the essential elements in nanotechnology due to their high surface-to-volume ratio, nanoscale size, and accompanying unique physicochemical properties.<sup>[1–3]</sup> Investigations regarding nanoparticles in research areas such as biosensing,<sup>[4]</sup> drug delivery,<sup>[5]</sup> catalysis,<sup>[6]</sup>

electronics,<sup>[7]</sup> and plasmonics<sup>[8,9]</sup> have enabled a variety of novel or improved applications. To open up more opportunities in nanotechnology, manipulating swarms of nanoparticles with precise spatial arrangement by bottom-up assembly has been identified as an important process where tailored nanoparticles become the building blocks of ordered systems.<sup>[10,11]</sup> Among nanoparticle surface assembly techniques, capillary-assisted particle assembly (CAPA) with predefined topographical templates has shown to be a promising method for the assembly of micro- or nanoscale objects on various surfaces.<sup>[12–14]</sup> For example, by utilizing funnel-shaped topographical assembly traps, deterministic position and orientation of assembled nanorods can be achieved.<sup>[15]</sup> Such trap engineering techniques make CAPA particularly advantageous for applications that rely on the precise positioning of hundreds or thousands of synthesized, highly crystalline nanoparticles,<sup>[16–18]</sup> to be used collectively as an array of nanoantennas<sup>[19,20]</sup> or to exploit plasmonic surface lattice resonances (SLR).<sup>[21,35,36]</sup> Furthermore, the integration with well-aligned micro- and nanoscale structures fabricated with top-down techniques is enabled by the accurate positioning of the assembled nanoparticles. As a result of this combination of top-down and bottom-up approaches, scalable production of advanced nanodevices such as electrically driven optical antennas<sup>[22,23]</sup> and tunneling nanogap electrodes<sup>[24,25]</sup> could be achieved. CAPA is a scalable process,<sup>[10,12,26,27]</sup> where a large batch of nanoparticles is assembled in parallel by a single step of a well-controlled capillary process. However, the fabrication of the topographical templates involves time-consuming processes such as electron beam lithography or other costly high-resolution photolithography processes. In most cases reported to date, the fabricated template can be used only a single time for the assembly. A strategy to improve the scalability and reduce costs is to reuse the templates. Various ideas to recycle CAPA templates have been reported, such as by transferring gold nanoparticles (AuNPs) from a silicon template onto a polydimethylsiloxane (PDMS) substrate via a dry peeling process,<sup>[28]</sup> or by replicating first the silicon template into PDMS or polymethylmethacrylate (PMMA), and performing CAPA on the PDMS or PMMA substrate for a subsequent transfer printing process.<sup>[29,30]</sup> By utilizing the dry peeling process, the transfer yield of the

H. S. C. Yu, A. Conde-Rubio, G. Boero, J. Brugger  
Microsystems Laboratory  
École Polytechnique Fédérale de Lausanne (EPFL)  
Lausanne CH-1015, Switzerland  
E-mail: juergen.brugger@epfl.ch

H.-C. Wang, O. J. F. Martin  
Nanophotonics and Metrology Laboratory  
École Polytechnique Fédérale de Lausanne (EPFL)  
Lausanne CH-1015, Switzerland

 The ORCID identification number(s) for the author(s) of this article can be found under <https://doi.org/10.1002/ppsc.202100288>.

© 2022 The Authors. Particle & Particle Systems Characterization published by Wiley-VCH GmbH. This is an open access article under the terms of the Creative Commons Attribution-NonCommercial License, which permits use, distribution and reproduction in any medium, provided the original work is properly cited and is not used for commercial purposes.

DOI: 10.1002/ppsc.202100288

assembled 60 nm AuNPs is reported to be 58%, however, the assembly position accuracy is not discussed.<sup>[28]</sup> By utilizing the transfer printing technique, the printing yield is reported to be 98.1%, however, the mean value of the printing accuracy for the 100 nm AuNPs is reported to be 60.8 nm.<sup>[30]</sup> A reusable assembly template that provides high accuracy of particle positioning as well as high particle transfer yield has not been reported yet.

Here, we demonstrate a fabrication process for reusable CAPA templates with funnel-shaped traps, which are designed for precise nanoparticle placement and high assembly yield. After chip-level CAPA processes with templates diced from the full wafer, the assembled AuNPs are transferred reliably from the reusable silicon assembly templates onto polymer substrates that are either stretchable PDMS (Sylgard 184, Dow Corning) or rigid OrmoComp (micro resist technology GmbH), respectively. Our work demonstrates the suitability of the proposed transfer and template reusability for future applications asking for different substrates.

## 2. Results and Discussion

### 2.1. Assembly Template Fabrication

The wafer-level fabrication process of assembly templates is compatible with standard cleanroom processes and is shown in **Figure 1**. A 130 nm thick SiO<sub>2</sub> thin film is deposited on a silicon wafer (100 mm diameter, P-doped) by plasma-enhanced chemical vapor deposition (PECVD). Vapor hexamethyldisilane is primed on the SiO<sub>2</sub> surface before the spin coating of ZEP-520A resist to increase the adhesion at the interface of SiO<sub>2</sub> and the resist, which determines the funnel sidewall angle. Circular openings with a diameter of about 100 nm in a 150 nm thick ZEP-520A resist are created by means of electron beam (e-beam) exposure and development. The subsequent O<sub>2</sub> plasma descumming process and buffered hydrofluoric acid wet etching create a vertically tapered funnel with sidewall angles of about 45°. After removing ZEP-520A resist by O<sub>2</sub> plasma ashing, anisotropic reactive

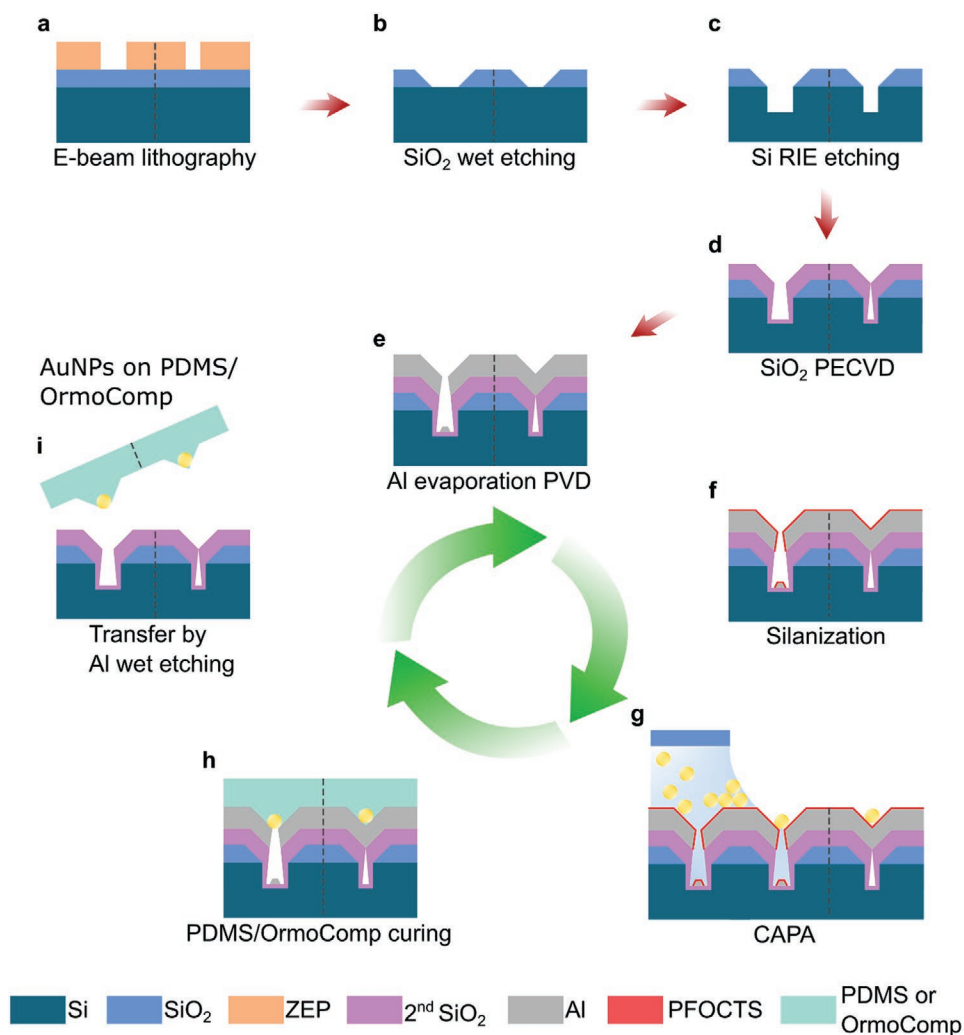


**Figure 1.** Scheme of the fabrication process flow of the reusable CAPA template with funnel (left half)- and cone (right half)-shaped traps. a–d) One-time-only processes. e–i) Cyclic processes to reuse the assembly template.

ion etching with  $\text{SF}_6/\text{C}_4\text{F}_8$  plasma using the patterned  $\text{SiO}_2$  layer as the hard mask is conducted to etch the silicon substrate, thereby creating the bottom part of the funnel, as shown in Figure 1c. The second  $\text{SiO}_2$  thin film with a thickness of 130 nm is then deposited by PECVD to narrow down the opening of the funnel neck, with a controllable sidewall deposition rate,<sup>[31]</sup> in order to prevent in the subsequent assembly that AuNPs are inserted into the funnel bottom. By reducing the diameter of the circular openings or increasing the thickness of the second  $\text{SiO}_2$ , the cone-shaped traps can be created with the trap neck that is clogged by the second  $\text{SiO}_2$  thin film, as shown in Figure 1d. A 150 nm thick aluminum thin film is then deposited by means of e-beam evaporation to serve as a sacrificial layer for the final wet etching transfer process (Figure 1e). The as-deposited aluminum surface becomes hydrophobic by exposure to  $\text{O}_2$  plasma and vapor-phase absorption of trichloro(1*H*,1*H*,2*H*,2*H*-perfluorooctyl)silane (PFOCTS, Sigma-Aldrich) under vacuum for 1.5 h (Figure 1f). The wettability of the aluminum surface is characterized through static contact angle measurements, obtaining values of about  $110^\circ$  with 3  $\mu\text{L}$  deionized (DI) water droplets at room temperature. Prior to the CAPA process, the wafer is mechanically diced into chips (about  $17 \times 17 \text{ mm}^2$ ). Detailed process parameters are listed in Table S1 (Supporting Information).

## 2.2. AuNP Assembly Yield and Position Offset

AuNPs with a diameter of 100 nm are assembled in arrays of cone-shaped and funnel-shaped traps with a pitch of 500 nm. To inspect the geometry of the traps, long trenches with analog dimensions to those of the traps are fabricated following the identical process and keeping the equal geometrical parameters. A diamond tip is used to cleave the sample and the cross-section is observed, shown in the scanning electron microscope (SEM) images in Figure 2a,b. The neck of the funnel-shaped trap has a width of 20–40 nm, as measured by SEM prior to the assembly process (Figure S1, Supporting Information). After CAPA, Figure 2c,d shows assembled AuNPs in two templates with funnel- and cone-shaped traps, respectively. The assembly yield, presented in Figure 2e, is obtained by sampling multiple arrays of 100 by 100 traps (10 000 traps) from the SEM images, for both funnel and cone templates. The comparably low percentage of empty traps (2.1% and 1.1%) suggests that the dynamics of particle insertion into the traps and resilience against the receding suspension front during the CAPA process are similar for both, funnel- and cone-shaped traps.<sup>[15]</sup> The difference in multiple particle assembly yields between the funnel and the cone template, as well as the large standard deviation of the multiple particle assembly yield, are presumably due to the variation of the meniscus contact angle during the CAPA

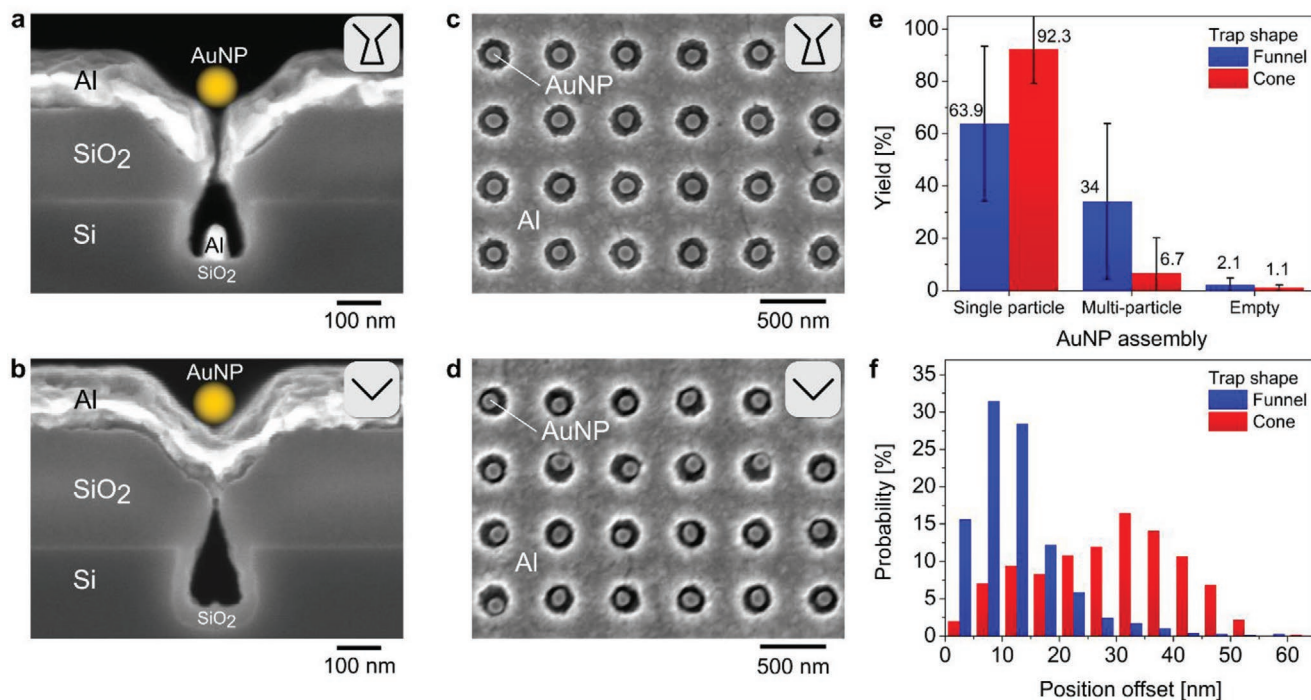


**Figure 2.** CAPA assembly results with traps of different shapes. a) SEM cross-sectional image of long rectangular trenches, serving as the structural references for the investigated circular funnel-shaped traps, and b) the circular cone-shaped traps (meaningful cross-sections of the circular traps cannot be effectively produced). The yellow dot is a sketch of a 100 nm AuNP, added to the SEM image as a dimensional reference in addition to the scale bar. The long rectangular trenches are fabricated using the identical process as the circular traps. c) SEM top-view image of an array of 100 nm diameter AuNPs assembled on the aluminum layer on a funnel template and d) on a cone template. e) Assembly yield statistics from multiple arrays of 10 000 traps sampled from the funnel and the cone templates, the error bars represent  $\pm 1\sigma$  among arrays (8 arrays for the funnel type and 10 arrays for the cone type). f) Probability distribution of the position offset of the assembled 100 nm AuNPs. 696 and 553 traps are sampled from the arrays with the highest single-particle yield (94% and 97%) from the funnel and the cone templates, respectively.

process, which is in the range of  $40^{\circ}$ – $55^{\circ}$ . In order to study the AuNP positioning accuracy in different trap shapes, a large trap diameter is adopted to allow significant position offsets. The large trap diameter also allows multiple particles to be inserted by higher downward capillary force when the meniscus contact angle becomes smaller as the AuNP accumulation zone grows over time during the CAPA process. This results in the relatively large variations of the multiple particle assembly yields among the studied arrays and templates. For the AuNP position offset analysis, an array from the funnel template with an assembly yield of 94% ( $\approx 2\%$  are empty and 4% contain more than one AuNP) is selected, and arrays from the cone template with an assembly yield of 97% ( $\approx 1\%$  are empty and 2% contain more than one AuNP) are selected. In particular, about 700 and 550 traps are sampled from the selected funnel and cone arrays, respectively. As shown in Figure 2f, the probability distribution of the position offset for AuNPs that are assembled in funnel traps is significantly different from that for AuNPs that are assembled in cone traps. The funnel template has a median position offset of 10 nm and a standard deviation of 8 nm, whereas the cone template has a median position offset of 30 nm and a standard deviation of 12 nm, respectively. The final position of particles assembled in topographical traps is predominantly affected by the capillary immersion force, which is present during the solvent drying stage after the meniscus is unpinned from the traps. In particular, assembled particles are driven by the capillary immersion force toward the edges or corners of the topographical trap provided that the trap bottom is

flat.<sup>[26,32]</sup> On the contrary, when using funnel traps, as depicted in Figure 1g, the volume below the neck of the funnel serves the purpose to accommodate the solvent (in our case  $0.3 \times 10^{-3}$  M cetyltrimethylammonium bromide, CTAB), which exerts an attraction force onto the assembled AuNP at the center of the trap during the drying stage, resulting in precise placement of the AuNP. Hence, we attribute the less precise centering of the AuNP in cone traps with respect to the funnel traps to the significantly different shape of the volume occupied by the solvent. The probability distribution of AuNP position offset in the cone traps spans from 0 nm (fixed at the center) to 70 nm (fixed at the edge) and has a peak at about 30 nm. Scatter plots of AuNP position vector are shown in Figure S2 (Supporting Information), and more statistical data are listed in Table S2 (Supporting Information).

### 2.3. AuNP Transfer

After SEM imaging of the assembled AuNPs on the CAPA templates for the yield and position offset analysis, the aforementioned funnel and cone templates are subjected to PDMS curing and aluminum wet etching processes (Figure 1h,i) in order to transfer the assembled AuNPs to PDMS substrates. The transfer yield is defined as the ratio of the number of AuNP transferred onto the PDMS substrate versus the number of assembled AuNP in a given array. The transfer yields are both larger than 99%, as determined by comparing the SEM images

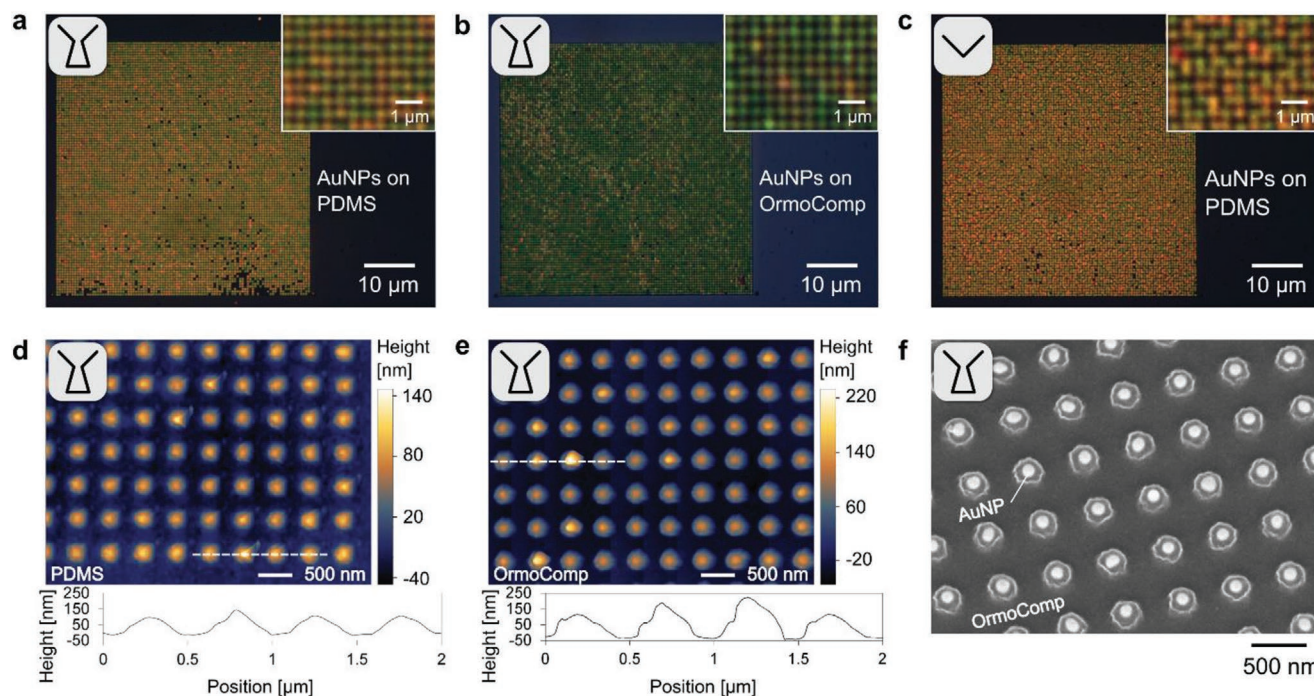


**Figure 3.** Results of the wet etching transfer processes of AuNPs on PDMS and OrmoComp substrates. a–c) Bright-field top-view optical microscope images of an AuNP array (100 by 100 with assembly and transfer yield loss) transferred from (a) a funnel template to a PDMS substrate, (b) a funnel template to an OrmoComp substrate, and (c) a cone template to a PDMS substrate. The insets are the corresponding magnified optical microscope images. These optical microscope images are acquired under identical microscope configurations. d,e) AFM images and topographic profiles of the arrays in (a) and (b), respectively. f) SEM image of the array in (b), with the sample tilted  $20^{\circ}$  and rotated (with 3 nm Cr coating). The arrays in (a) and (c) are the arrays studied in Figure 2f.

of the assembled AuNPs and the optical microscope (OM, Leica DM800) images acquired under the identical OM configuration from both PDMS substrates (Figure 3a,c). Each of the bright dots in the OM images represents single or multiple AuNP in one trap. From the magnified OM images shown as insets, the significant difference in position offset of AuNPs between the funnel (Figure 3a) and the cone (Figure 3c) templates can be still seen after the wet etching transfer processes. The difference in color among bright dots is mainly due to the variation in the AuNP size, aspect ratio, and the number of AuNP in one trap, which leads to localized surface plasmon resonance (LSPR) peaks at different wavelengths within the visible light range. The high transfer yield is achieved, thanks to the use of the aluminum sacrificial layer,<sup>[33]</sup> which is chemically etched during the wet etching transfer process to release AuNPs from the assembly template. In contrast to the dry peeling transfer process reported previously,<sup>[28]</sup> the wet etching transfer process does not apply any mechanical normal and shear stress at the interfaces of AuNPs and the PDMS substrate, which allows for more successful transfer of the AuNPs. To highlight the applicability of the method proposed in this work to different substrates, in addition to PDMS substrates, AuNPs assembled on a funnel template are transferred also to an OrmoComp substrate, which is a glass-like, UV-curable rigid and transparent polymer. The transfer yield to OrmoComp is also larger than 99%, as shown in Figure 3b. The difference in the refractive index of OrmoComp ( $\approx 1.52$ ) and PDMS ( $\approx 1.4$ ) results in the color difference of AuNPs on the OrmoComp (Figure 3b) and the PDMS (Figure 3a,c) substrates. To further investigate the surfaces of substrates after the wet etching transfer processes, atomic force microscope (AFM) images are taken from the funnel traps on PDMS and OrmoComp substrates, as shown in Figure 3d,e, respectively. The dimensions of the funnel traps on both assembly templates were designed to be identical. Nevertheless, the maximum peak height and the deviation in peak heights (the negative of funnels) of the OrmoComp substrate are larger than those of the PDMS substrate. This is presumably due to the differences in material preparation and the viscosity of PDMS and OrmoComp. On one hand, OrmoComp is poured on a funnel template and degassed as-purchased with a nominal viscosity of  $2.0 \pm 0.5$  Pa s. During the degassing process, the uncured OrmoComp flows into the bottom part of funnel traps through the neck and the aluminum sacrificial layer under assembled AuNPs, resulting in large and diversified topographic peak heights. After UV curing and the wet etching transfer process, the cured OrmoComp residues left in funnel traps on the assembly template are observed in SEM images, as shown in Figure S3a (Supporting Information). On the other hand, uncured PDMS is prebaked at 80 °C for 7 min, which not only partially cures PDMS to increase the viscosity to about 8 Pa s, but also accelerates the PDMS curing at room temperature.<sup>[34]</sup> This pretreatment prevents PDMS from flowing through the funnel necks before reaching the gel point, i.e., losing fluidity, without compromising the fidelity of topographic replication and the AuNP transfer yield. As a result, the funnel assembly template subjected to the wet etching transfer process with prebaked PDMS is residue-free in traps, as shown in Figure S3b (Supporting Information). Since no material contrast is visible in the AFM images (Figure 3d,e),

SEM images are acquired after the wet etching transfer process, as shown in Figure 3f and Figure S4 (Supporting Information), to reveal AuNPs embedded in OrmoComp, showing that the positions of AuNPs are maintained after the wet etching transfer process. We also characterize the optical response of the transferred AuNP arrays on PDMS substrates by collecting the optical reflectance spectra under normal incidence, as shown in Figure S5a (Supporting Information). The arrays of 100 nm AuNP show a broad peak at 585 nm assigned to the LSPR. The SLR mode, characteristic of plasmonic arrays, is not visible. According to simulations done with COMSOL (COMSOL Inc.), the SLR mode is weak and overlapping with the LSPR. This particle size is chosen for the ease of measuring the position offset. Arrays of bigger nanoparticles present a visible peak corresponding to the SLR. As the SLR is directly linked to the pitch in the array, this optical characterization method could give information about the quality of the array in terms of pitch variations. As an example, we use 200 nm AuNPs and assemble them with a pitch of 500 nm. In this case, we observe a broad shoulder around 600–650 nm and a peak at 716 nm (709 nm in the performed simulation), that is assigned to the SLR (Figure S5, Supporting Information).

Among the different approaches to recycle CAPA templates,<sup>[28–30,35,36]</sup> assembly areas up to  $1 \text{ cm}^2$  on PDMS substrates are reported using the mold replication technique.<sup>[35]</sup> In our work, the dimension of the assembly area in the direction of meniscus moving is currently limited to a few millimeters in size. However, our process allows to transfer the assembled AuNPs not only onto elastomer substrates such as PDMS ( $E = 1200$  kPa) but also onto rigid substrates such as OrmoComp ( $E = 1$  GPa). The versatility demonstrated here is not straightforward to be achieved in mold replication or dry peeling processes due to the requirement for substrate flexibility. Besides, the use of an aluminum sacrificial layer is more convenient when a combination of top-down and bottom-up approaches is desired (e.g., adding electrical contacts to assembled particles).

#### 2.4. The Reusability of Assembly Templates

After the transfer of the assembled AuNPs onto PDMS substrates, the funnel template (Figure 2c) and the cone template (Figure 2d) are reused for subsequent assembly processes by repeating the processes illustrated in Figure 1e–g. The results are shown in Figure 4. The average percentage of empty traps with the reused funnel template is 8%, and the standard deviation is 4% (Figure 4a), whereas the average percentage of empty traps with the reused cone template is 4%, and the standard deviation is 3% (Figure 4b). Both reused templates show low percentages of empty traps but slightly higher than that of the first-time used templates (Figure 2e). This difference is presumably due to the known CAPA process-to-process variations. The large standard deviations of the multiple particle assembly yields (10% for the funnel template and 36% for the cone template) are due to the reason aforementioned. The probability distributions of AuNP position offset are comparable between first- and second-time used templates, as shown in Figure 4c,d, regardless of the shape of traps. The reused funnel template has a median position offset of 10 nm and a standard deviation

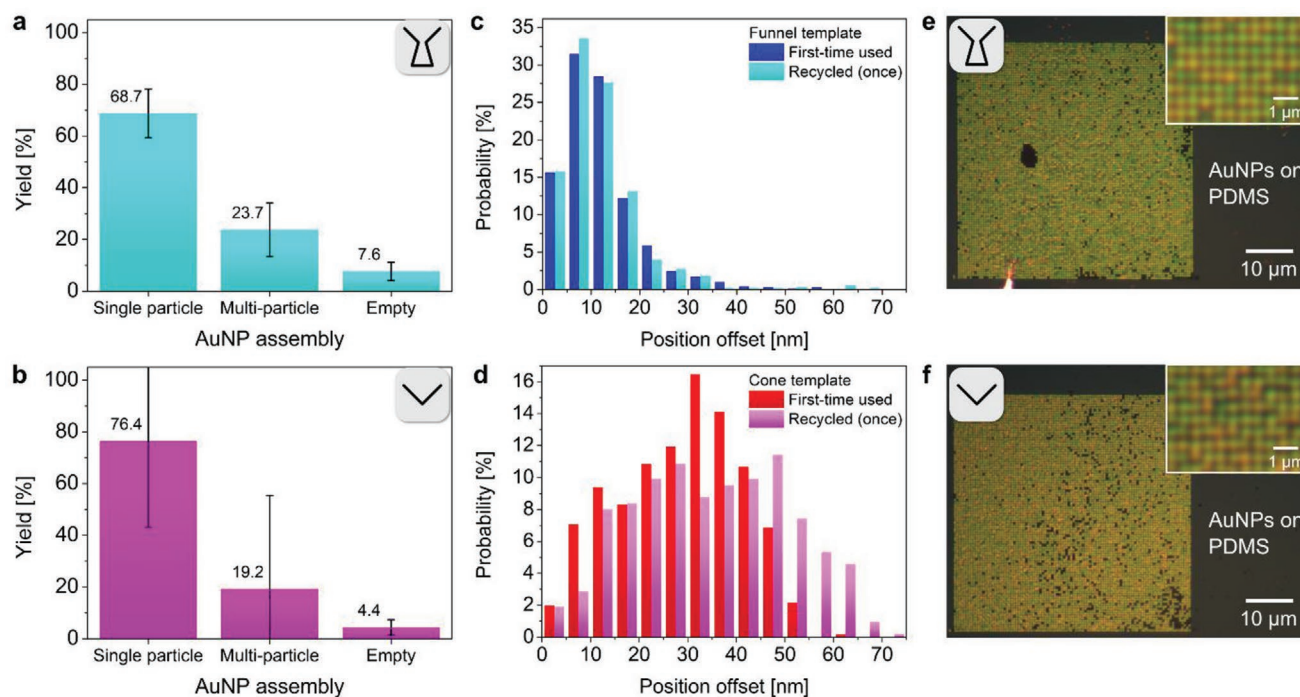


**Figure 4.** CAPA assembly template reusability. a) Assembly yield statistics of multiple arrays of 10 000 traps sampled from the reused funnel template and b) the reused cone template. The error bars represent  $\pm 1\sigma$  among arrays (5 arrays for the funnel type and 4 arrays for the cone type). c) Comparison of the probability distribution of AuNP position offset. 558 traps are sampled from the same array in Figure 2f on the reused funnel template and d) 526 traps from the same arrays in Figure 2f on the reused cone templates. e) Bright-field top-view optical microscope images of an AuNP array transferred from the reused funnel template to a PDMS substrate, and f) from the reused cone template to a PDMS substrate. The insets are the corresponding magnified optical microscope images. These optical microscope images are acquired under an identical microscope configuration.

of 9 nm, whereas the reused cone template has a median position offset of 35 nm and a standard deviation of 16 nm. An irregular pinning in the funnel array sampled for Figure 4c is observed during the CAPA process and the assembly is not completed for the entire array (see Figure S7a in the Supporting Information). This is probably linked to the microscale local inhomogeneity of PFOCTS molecules' absorption on the template surface. Therefore, the assembly result from this array is only used for position offset analysis and is not included in the assembly yield statistics of the reused funnel template. The assembled AuNP arrays on the reused templates are also transferred to PDMS substrates by the wet etching transfer process. The OM images of AuNP arrays on PDMS substrates show wet etching transfer yields larger than 99% with both the reused funnel template (Figure 4e) and the reused cone template (Figure 4f). A SEM image of the reused funnel template after the second-time wet etching transfer process is shown in Figure S7b (Supporting Information).

### 3. Conclusion and Outlook

In this work, we demonstrate a process to fabricate reusable templates for precise nanoparticle placement with the CAPA technique and show a systematic yield study of the assembly and transfer step. The assembly yield with arrays of  $\approx 10\,000$  funnel traps is as high as 94% with a median particle position offset in the order of 10 nm. Cone traps achieve a similar maximum

assembly yield of 97% but have a larger median position offset of 30 nm. The assembled AuNPs are then transferred from the assembly template onto PDMS and OrmoComp substrates with transfer yields larger than 99%. To enable the reusability of the template, a pretreatment of uncured PDMS is a prerequisite to ensure a residue-free assembly template after the wet etching transfer process. The result of the yield and position offset of AuNPs assembled using the recycled template is comparable to that of the first use, demonstrating that the proposed process allows for the fabrication of reusable templates.

The process presented here also paves the way for the precise positioning of thousands of bottom-up assembled nanoparticles with precise alignment to top-down fabricated micro- or nanostructures, and therefore enables integrated nanosystems made of lithography-defined patterns and template assembly. The presented process allows in particular the scalable fabrication of advanced nanodevices such as electrically driven optical antennas and tunable tunneling nanogap electrodes and might ultimately facilitate applications in nanolight sources and single-molecule detection, which remain a challenge for the present cutting-edge transfer printing and dry peeling transfer techniques.

### 4. Experimental Section

*Nanoparticle Assembly:* The procedures for nanoparticle preparation and assembly followed a method that is detailed elsewhere.<sup>[15]</sup> An image

of the custom-made setup for CAPA processes is shown in Figure S8 (Supporting Information). Spherical AuNPs with a nominal diameter of 100 nm stabilized with an adsorbed monolayer of CTAB (Nanopartz, USA) were suspended in  $0.3 \times 10^{-3}$  M CTAB solution (in DI water). 120  $\mu$ L of AuNP solution was dispensed into a 1.8 mm separation between the template and the upper glass coverslip. The template temperature was typically set to 45–48 °C to accelerate the accumulation zone formation and the template was moved by a motorized linear translation stage (PI miCos, PLS-85) at a speed of  $1.2 \mu\text{m s}^{-1}$ . The initial position of the meniscus was set to be 1.5 mm away from the edge of the trap area to have  $\approx 20$  min preconditioning time and to achieve stable AuNP accumulation prior to crossing over the trap arrays. Figure S9 (Supporting Information) shows the statistical analysis of the diameter of the AuNPs and the funnel traps, respectively. The AuNPs had a mean diameter of 112 nm and a standard deviation of 6 nm, whereas the funnel traps had a mean diameter of 220 nm and a standard deviation of 6 nm.

**AuNP Wet Etching Transfer and Template Recycle:** After the assembly of the 100 nm AuNPs, as shown in Figure 1g, the assembly templates with the AuNPs were treated with  $\text{O}_2$  plasma (Tepla 300) to remove the exposed CTAB layer covering the AuNPs. The templates with the AuNPs were subsequently immersed in (3-mercaptopropyl)trimethoxysilane solution (MPTMS, Sigma-Aldrich) for 2 h and rinsed with isopropyl alcohol to assemble MPTMS on the surfaces of the AuNPs as an adhesive layer.<sup>[33]</sup> The template with the assembled AuNPs was then covered by a liquid polymer that was poured over the surface followed by curing. Two polymer variations were studied: first, partially cured 10:1 PDMS ( $\approx 22$  g, 80 °C, 7 min prebaking) was poured, degassed for 1 h, and cured at room temperature for a total time of 48 h in order to avoid thermal stress. Second, UV-curable OrmoComp was poured, degassed for 1 h, and cured at room temperature by exposure to UV radiation (375 nm,  $2.5 \text{ mW cm}^{-2}$ ) for 30 s. The thickness of the cured films of PDMS and OrmoComp were about 3 and 1 mm, respectively. The sample was immersed in a diluted hydrochloric acid bath to etch the aluminum thin sacrificial film for a time ranging from 12 to 72 h, until the cured PDMS or OrmoComp substrates were separated from the  $\text{SiO}_2$  surface together with the assembled AuNPs. After the wet etching transfer process of the AuNPs, the assembly templates were ready to be reused by repeating the cyclic processes, as shown in Figure 1e–i. Detailed process parameters are listed in Table S3 (Supporting Information).

**Assembly Yield and Position Offset Analysis:** The assembly yield is defined as the ratio of the number of traps filled with a single AuNP versus the total number of traps of the given array, as imaged in the SEM (Zeiss Merlin). Assembly yield images were recorded with a resolution of 21.7 nm per pixel from corners of arrays, containing about 1200 traps in each image. The position offset is defined as the distance between the centroids of an assembled AuNP and the corresponding trap. The coordinates of centroids were extracted from postprocessed SEM images by ImageJ software (v1.53e). A total number of 8 SEM images for a position offset analysis were recorded with a resolution of 10.9 nm per pixel and postprocessed by MATLAB software (R2017b) to correct the unavoidable sample tilting due to manual sample mounting on the SEM stage. SEM images for both assembly yield and position offset analysis were acquired at 3 kV and 400 pA probe current using either InLens or HE-SE2 secondary electron detectors to provide material contrast sufficient to distinguish the AuNPs from the aluminum surface and trap topography. To evaluate the reusability of the assembly template, two templates were prepared, one with funnel-shaped traps and one with cone-shaped traps.

**Analysis of PDMS/OrmoComp Substrates with Transferred AuNPs:** The topographic study was done by scanning the PDMS and the OrmoComp substrate surfaces with an AFM (Bruker Dimension FastScan, ScanAsyst mode) after the wet etching transfer process. The topographic data were postprocessed by Gwyddion software (64 bit v2.49) for the leveling. The SEM (Zeiss Merlin) images of the OrmoComp substrate (with 3 nm Cr coating) were acquired at 10 kV and 400 pA probe current using InLens secondary electron detectors to provide material contrast sufficient to distinguish the AuNPs from the OrmoComp surface. SEM imaging of

AuNPs assembled on PDMS did not result in high-quality microscopy images because the energetic electrons which provided material contrast tended to damage the PDMS substrate. Therefore, only OM and AFM images were shown.

## Supporting Information

Supporting Information is available from the Wiley Online Library or from the author.

## Acknowledgements

The authors would like to thank the colleagues from the Center of MicroNanoTechnology (CMi) in EPFL. Most of the fabrication processes in this work were done in the CMi with supports from CMi staff and experts. The authors would also like to thank Dr. Mohammadmehdi Kiaee (Microsystems laboratory, EPFL) for his support in rheology studies of the wet etching transfer processes. This work has received funding from the European Research Council (ERC) under the European Union's Horizon 2020 research and innovation program (Grant No. ERC-2016-ADG, Project "MEMS 4.0" Grant No. 742685), and funding from the European Research Council (Grant No. ERC-2015-AdG-695206 Nanofactory).

Open access funding provided by Ecole Polytechnique Federale de Lausanne.

## Conflict of Interest

The authors declare no conflict of interest.

## Data Availability Statement

The data that support the findings of this study are available from the corresponding author upon reasonable request.

## Keywords

capillary-assisted particle assembly, funnel assembly traps, precise placement, reusable templates

Received: December 27, 2021

Revised: January 24, 2022

Published online: February 8, 2022

- [1] I. Khan, K. Saeed, I. Khan, *Arabian J. Chem.* **2019**, *12*, 908.
- [2] M. Auffan, J. Rose, J. Y. Bottero, G. V. Lowry, J. P. Jolivet, M. R. Wiesner, *Nat. Nanotechnol.* **2009**, *4*, 634.
- [3] E. Roduner, *Chem. Soc. Rev.* **2006**, *35*, 583.
- [4] L. Dykman, N. Khlebtsov, *Chem. Soc. Rev.* **2012**, *41*, 2256.
- [5] J. Panyam, V. Labhasetwar, *Adv. Drug Delivery Rev.* **2012**, *64*, 61.
- [6] C. J. Jia, F. Schüth, *Phys. Chem. Chem. Phys.* **2011**, *13*, 2457.
- [7] J. E. Millstone, D. F. J. Kavulak, C. H. Woo, T. W. Holcombe, E. J. Westling, A. L. Briseno, M. F. Toney, J. M. J. Fréchet, *Langmuir* **2010**, *26*, 13056.
- [8] S. Gwo, H.-Y. Chen, M.-H. Lin, L. Sun, X. Li, *Chem. Soc. Rev.* **2016**, *45*, 5672.
- [9] N. J. Halas, S. Lal, W. S. Chang, S. Link, P. Nordlander, *Chem. Rev.* **2011**, *111*, 3913.
- [10] J. Yin, Y. Huang, S. Hameed, R. Zhou, L. Xie, Y. Ying, *Nanoscale* **2020**, *12*, 17571.

- [11] M. Grzelczak, J. Vermant, E. M. Furst, L. M. Liz-Marzán, *ACS Nano* **2010**, *4*, 3591.
- [12] S. Ni, L. Isa, H. Wolf, *Soft Matter* **2018**, *14*, 2978.
- [13] Y. Yin, Y. Lu, B. Gates, Y. Xia, *J. Am. Chem. Soc.* **2001**, *123*, 8718.
- [14] Y. Xia, Y. Yin, Y. Lu, J. McLellan, *Adv. Funct. Mater.* **2003**, *13*, 907.
- [15] V. Flauraud, M. Mastrangeli, G. D. Bernasconi, J. Butet, D. T. L. Alexander, E. Shahrabi, O. J. F. Martin, J. Brugger, *Nat. Nanotechnol.* **2016**, *12*, 73.
- [16] J. H. Park, P. Ambwani, M. Manno, N. C. Lindquist, P. Nagpal, S. H. Oh, C. Leighton, D. J. Norris, *Adv. Mater.* **2012**, *24*, 3988.
- [17] M. Kuttge, E. J. R. Vesseur, J. Verhoeven, H. J. Lezec, H. A. Atwater, A. Polman, *Appl. Phys. Lett.* **2008**, *93*, 113110.
- [18] H. Ditlbacher, A. Hohenau, D. Wagner, U. Kreibig, M. Rogers, F. Hofer, F. R. Aussenegg, J. R. Krenn, *Phys. Rev. Lett.* **2005**, *95*, 257403.
- [19] C. Huang, A. Bouhelier, G. Colas Des Francs, A. Bruyant, A. Guenot, E. Finot, J. C. Weeber, A. Dereux, *Phys. Rev. B: Condens. Matter Mater. Phys.* **2008**, *78*, 155407.
- [20] F. Timpu, N. R. Hendricks, M. Petrov, S. Ni, C. Renaut, H. Wolf, L. Isa, Y. Kivshar, R. Grange, *Nano Lett.* **2017**, *17*, 5381.
- [21] Y. Brasse, V. Gupta, H. C. T. Schollbach, M. Karg, T. A. F. König, A. Fery, *Adv. Mater. Interfaces* **2020**, *7*, 1901678.
- [22] J. Kern, R. Kullock, J. Prangma, M. Emmerling, M. Kamp, B. Hecht, *Nat. Photonics* **2015**, *9*, 582.
- [23] R. Kullock, M. Ochs, P. Grimm, M. Emmerling, B. Hecht, *Nat. Commun.* **2020**, *11*, 5.
- [24] Y. Cui, M. T. Björk, J. A. Liddle, C. Sönnichsen, B. Boussert, A. P. Alivisatos, *Nano Lett.* **2004**, *4*, 1093.
- [25] H. S. Yu, G. Boero, J. Brugger, in *TRANSDUCERS EUROSENSORS XXXIII*, IEEE, Berlin, Germany **2019**, p. 2368.
- [26] S. Ni, M. J. K. Klein, N. D. Spencer, H. Wolf, *Langmuir* **2014**, *30*, 90.
- [27] M. Asbahi, S. Mehraeen, F. Wang, N. Yakovlev, K. S. L. Chong, J. Cao, M. C. Tan, J. K. W. Yang, *Nano Lett.* **2015**, *15*, 6066.
- [28] K. Sugano, T. Ozaki, T. Tsuchiya, O. Tabata, *Sens. Mater.* **2011**, *23*, 263.
- [29] T. Kraus, L. Malaquin, H. Schmid, W. Riess, N. D. Spencer, H. Wolf, *Nat. Nanotechnol.* **2007**, *2*, 570.
- [30] J. B. Lee, H. Walker, Y. Li, T. W. Nam, A. Rakovich, R. Sapienza, Y. S. Jung, Y. S. Nam, S. A. Maier, E. Cortés, *ACS Nano* **2020**, *14*, 17693.
- [31] T. S. Cale, *J. Vac. Sci. Technol., B: Microelectron. Nanometer Struct.–Process., Meas., Phenom.* **1990**, *8*, 1242.
- [32] M. J. Gordon, D. Peyrade, *Appl. Phys. Lett.* **2006**, *89*, 053112.
- [33] E. K. W. Tan, G. Rughoobur, J. Rubio-Lara, N. Tiwale, Z. Xiao, C. A. B. Davidson, C. R. Lowe, L. G. Occhipinti, *Sci. Rep.* **2018**, *8*, 6607.
- [34] E. J. Wong, *Doctoral Thesis*, Massachusetts Institute of Technology **2010**.
- [35] M. Juodenas, T. Tamulevičius, J. Henzie, D. Erts, S. Tamulevičius, *ACS Nano* **2019**, *13*, 9038.
- [36] M. Juodenas, D. Peckus, T. Tamulevičius, Y. Yamauchi, S. Tamulevičius, J. Henzie, *ACS Photonics* **2020**, *7*, 3130.